Journal of Materials Science: Materials in Electronics (2019) 30:1282–1291
https://doi.org/10.1007/s10854-018-0396-z

Improved thermoelectric properties of n-type Bi_2Te_3 alloy deriving from two-phased heterostructure by the reduction of CuI with Sn

Mi-Kyung Han[1] · Junphil Hwang[1] · Sung-Jin Kim[1]

Received: 24 October 2018 / Accepted: 15 November 2018 / Published online: 28 November 2018

Abstract

In this report, CuI and Sn co-doped n-type Bi_2Te_3 samples have been prepared by a high-temperature solid-state reaction, and the effect of co-doping on the thermoelectric properties was investigated from room temperature to 525 K. Sn single-doped and undoped Bi_2Te_3 were prepared for comparison. Detailed charge transport data including electrical conductivity, Seebeck coefficient, Hall coefficient, and thermal conductivity are presented. Microscopic observation of CuI/Sn co-doped samples revealed that numerous distinctive microstructures such as nanoprecipitates of the Cu and SnI-rich phase were generated in the matrix. The lattice thermal conductivity of CuI/Sn co-doped Bi_2Te_3 was substantially reduced compared to those of undoped and single doped Bi_2Te_3. Benefiting from the improved electrical transport properties by doping and the reduced lattice thermal conductivity by numerous microstructures, the ZT value of the Bi_2Te_3 doped with 1 at.% CuI/Sn is distinctly enhanced to 1.24 at 425 K. The average ZT value (ZT_{ave} ~ 1.02) at 300–525 K was clearly higher than those of Sn-doped Bi_2Te_3 (ZT_{ave} ~ 0.54) and CuI-doped Bi_2Te_3 (ZT_{ave} ~ 0.98). This work indicates that the average ZT can be improved over a broad temperature range using a co-doping approach.

1 Introduction

Thermoelectric materials, which can enable direct transformation of waste heat to electric energy, provide an alternative solution to energy and environmental issues. Thus, exploring high-efficiency thermoelectric materials have attracted ever-increasing attention both from the viewpoint of an academic research and industrial applications [1, 2]. The efficiency of a thermoelectric device is directly related to the material's thermoelectric performance, which is determined by a dimensionless figure of merit (ZT), defined as $ZT = (S^2\sigma/\kappa)T$, where S, σ, κ and T denote the Seebeck coefficient, electrical conductivity, thermal conductivity and working temperature in Kelvin, respectively [3].

Bismuth telluride (Bi_2Te_3) and its alloys are regarded as some of the most promising materials for solid-state refrigeration applications, and they operate in a temperature range between 200 and 400 K [4]. A series of p- and n-type semiconductor pairs are needed to fabricate the thermoelectric cooling devices [5]. A high ZT of > 1.86 at 320 K was achieved in p-type Bi_2Te_3-based TE materials [6]. However, the ZT value of n-type Bi_2Te_3 is still relatively lower than that of its p-type counterpart [7–9]. Therefore, there is still a great need for developing new n-type Bi_2Te_3 with a high ZT that can match well with p-type counterparts. So far, considerable efforts have been made to enhance the thermoelectric properties of n-type Bi_2Te_3 by changing its composition by chemical doping/alloying [10–13], and microstructural modification by introducing defects/nanostructures [7, 14, 15]. Bi_2Te_3 can be p-type by doping with extrinsic atoms such as Bi, Se, Ge, Sn, Pb, and rare earth elements or n-type with In, Cl, I, CuI, and SbI_3 [16]. The resonant level formed by Sn doping strongly enhances the thermoelectric power of Bi_2Te_3 at room temperature [17]. Intercalation of metal between the weak van der Waals gap in the Bi_2Te_3 structure has been realized one of the effective strategy to improve the ZT value and stability of Bi_2Te_3 materials [18–20]. However, it is very difficult to achieve high levels of intercalation due to the formation of secondary phases or substitution instead of intercalation by interactions between intercalant species and the matrix. Combining the effects of substitution and intercalation has also been reported previously to improve the thermoelectric properties [21]. The co-doping of Cu and I in Bi_2Te_3 enhances the power factor, thus increasing the ZT of $(CuI)_{0.01}$ Bi_2Te_3 (ZT ~ 1.16 at 368 K). In addition to

✉ Sung-Jin Kim
sjkim@ewha.ac.kr

1 Department of Chemistry and Nano Science, Ewha Womans University, Seoul 120-750, Republic of Korea

the high peak ZT, thermoelectric materials should also have high average performance within the working temperature range.

Herein, we report new progress in tuning the thermoelectric properties of n-type Bi_2Te_3 by employing CuI as a co-dopant with Sn. The experiment was conducted in two stages. We first studied the effect of the concentration of the alloyed Sn atoms on the thermoelectric properties of Bi_2Te_3. After this, we carried out experiments on co-doping; more specifically, we studied the variation of the thermoelectric properties of Bi_2Te_3 doped with both Sn and CuI.

2 Materials and methods

2.1 Synthesis

All reagents were purchased from Sigma-Aldrich and were used as obtained including: Bi chunks (99.999%), Te chunks (99.999%), CuI powder (99.999%), and granular Sn (99.5%). A series of CuI/Sn co-doped Bi_2Te_3 samples with a chemical formula of $(CuI+1/2Sn)_xBi_{2-x}Te_3$ (x = 0.01, 0.03, 0.05, 0.07, 0.1; namely CuI/Sn-substituted Bi_2Te_3) and $(CuI+1/2Sn)_xBi_2Te_3$ (x = 0.01, 0.03, 0.05, 0.07, 0.1; namely CuI/Sn-added Bi_2Te_3) were prepared by means of the conventional high-temperature solid-state reaction method. Bi_2Te_3 samples doped by Sn alone with the chemical formulas $Sn_xBi_{2-x}Te_3$ (x = 0.01, 0.03, 0.05; namely Sn-added Bi_2Te_3) and $Bi_{2-x}(Sn)_xTe_3$ (x = 0.01, 0.03, 0.05; namely Sn-substituted Bi_2Te_3) were prepared under identical experimental conditions to allow for a meaningful comparison. We also prepared undoped Bi_2Te_3 as a pristine material. A series of doped Bi_2Te_3 samples with masses of ~ 30 g were melted in evacuated quartz tubes (~ 10^{-3} Torr) using a rocking furnace at 1273 K for 24 h; then, the samples were cooled to room temperature at a rate of 80 °C h^{-1}. The resulting ingots were crushed into fine powders using a ball mill (8000D; SPEX, USA) for 40 min. Then, the samples were densified by a spark plasma sintering (SPS) method (SPS-211LX, Fuji Electronic Industrial Co., Ltd.) at 723 K for 5 min in a 12.7 mm diameter graphite die under an axial compressive stress of 50 MPa in vacuum. Highly densified (> 98% of theoretical density) disk-shaped pellets were obtained.

2.2 Characterization of materials

The main paragraph text follows directly on here. Powder diffraction patterns were obtained with Cu Kα (λ = 1.5418 Å) radiation in a reflection geometry on a diffractometer operating at 40 KV and 30 mA equipped with a position sensitive detector. The lattice parameters were obtained by a least squares refinement of the data in the 2θ range of 10°–70° with the assistance of a Rietveld refinement program [22]. Room temperature Hall coefficients (R_H) were measured using a Hall effect measurement system (HT-Hall, ResiTest 8300, Toyo Corporation). Carrier density (n_H) was obtained by $n_H = 1/(eR_H)$, and carrier mobility (μ_H) was calculated using the relationship $\mu_H = \sigma R_H$, where σ is the electrical conductivity obtained from ZEM-3 instrument and *e* is the free electron charge. Microstructures were investigated by transmission electron microscopy (HRTEM, JEM-2100F).

2.3 Characterization of TE properties

The obtained spark plasma sintering (SPS) processed pellets were cut into bars with dimensions of $12 \times 3 \times 3$ mm^3 for the simultaneous measurement of the Seebeck coefficient and electrical conductivity using an Ulvac Riko ZEM-3 instrument under a low-pressure inert gas (He) atmosphere from room temperature to 520 K. The uncertainties in the Seebeck coefficient and electrical conductivity measurement were ± 8% and ± 10%, respectively. The SPSed pellets were cut and polished into a round shape of Φ 15 mm × 2 mm for thermal diffusivity (D) and specific heat capacity (C_p) measurements in a Netzsch LFA457 MicroFlash™ instrument. The samples were coated with a thin layer of graphite to minimize errors from the emissivity method. The density (ρ) was determined using the dimensions and mass of the sample. Thermal conductivity (κ_{tot}) can be derived from the relationship $\kappa_{tot} = D \times C_{p \times} \rho$. The uncertainty in the thermal conductivity was estimated to be about ± 10%, considering all the uncertainties from D, ρ and C_p. The combined uncertainty for all measurements involved in the calculation of ZT was less than 15%. Unless otherwise noted, all the properties described in this study were measured perpendicular to the sintering pressure direction.

3 Results and discussion

Figure 1 shows the XRD patterns of single Sn-doped and CuI/Sn co-doped Bi_2Te_3. All the main peaks of the samples can be well indexed to the phase of Bi_2Te_3 (JCPDS ICDD 2002 #89-2009) [23], and no obvious impurity phases were observed. No significant peak shifts were observed within the composition range for either the Sn or CuI/Sn doped samples. The lattice parameter *a* (4.37(1) Å) was almost the same for all compounds, while the lattice parameter *c* was 30.48(1) Å for the pristine compound, 30.49(1) Å for 1 at.% Sn-added, 30.48 (1) Å for 1 at.% Sn-substituted, 30.45(1) Å for 1 at.% CuI/Sn-added and 30.34(1) Å for 1 at.% CuI/Sn-substituted Bi_2Te_3. These values slightly decreased with CuI /Sn co-doping.

According to the Lotgering method [24], the relative peak intensity ratio of the (006)–(015) peaks, $I_{(006)}/I_{(015)}$, was about ~ 0.18 for the Sn-doped Bi_2Te_3 sample and ~ 0.10

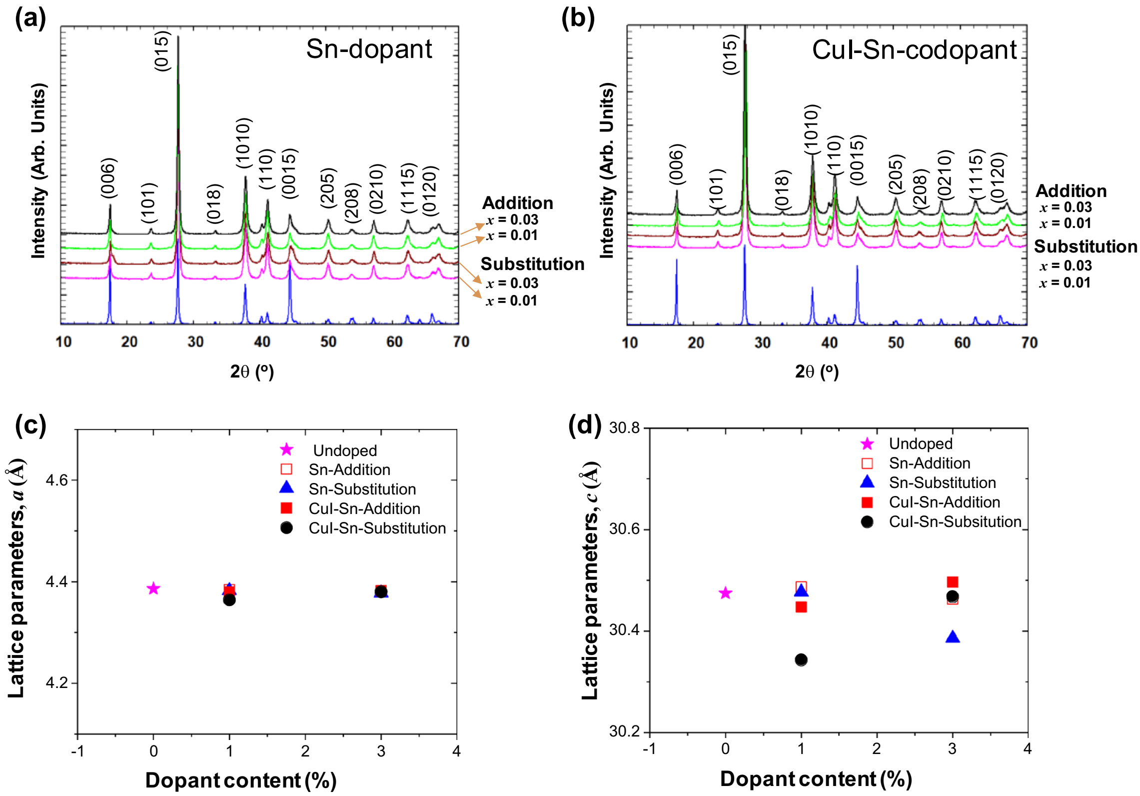

Fig. 1 **a** Powder XRD patterns for $Sn_xBi_2Te_3$and $Bi_{2-x}Sn_xTe_3$ (x = 0.0, 0.01, 0.03). **b** Powder XRD patterns for $(CuI + 1/2Sn)_xBi_2Te_3$ and $Bi_{2-x}(CuI + 1/2Sn)_xTe_3$ (x = 0.0, 0.01, 0.03), **c** lattice parameter a, **d** lattice parameter c

for CuI/Sn co-doped Bi_2Te_3, indicating no obvious preferred orientation in these samples. All the samples showed a dense structure (the relative density reached 98%), thus we paid little attention to the porosity and anisotropy when analyzing the thermoelectric properties.

Hall measurements were carried out at room temperature to estimate the carrier concentration of different doping types and content in Bi_2Te_3. The resulting carrier concentration n_H and mobility μ_H are listed in Table 1. First of all, we noted that the carrier concentration in the undoped Bi_2Te_3 samples was approximately $n \approx 1.2 \times 10^{19}$ cm^{-3}. When doping with CuI, the carrier concentration slightly increased because parts of the Cu and I atoms dissolved into the matrix as the electron donors ($n \approx 5.9 \times 10^{19}$ cm^{-3}). Generally, Sn is known to act as an electron acceptor by the substitution of divalent Sn^{2+} for trivalent Bi^{3+} in Bi_2Te_3, thus compensating for the electron carriers. The concentration of holes from Sn doping surpassed that of majority carriers in pristine Bi_2Te_3 by increasing the amount of Sn to 3 at.%, and noticeable changes in the conduction type were detected. The 3 at.% Sn-doped samples (both substituted and intercalated Bi_2Te_3) show p-type conduction ($p \approx 2 \times 10^{19}$ cm^{-3}for $Sn_{0.03}Bi_2Te_3$, and $p \approx 3 \times 10^{19}$ cm^{-3} for $Sn_{0.03}Bi_{1.97}Te_3$). The samples with low Sn contents showed complicated behavior.

Table 1 Properties of Sn-doped, CuI-doped and CuI/Sn co-doped Bi_2Te_3 at 300 K compared with pristine Bi_2Te_3

Sample	Type	Carrier concentration (10^{19} cm^{-3})	Mobility (cm^2 V^{-1} s^{-1})
$Bi_2Te_3(CuI)_xBi_2Te_3$	n	1.2	355
x = 0.01	n	5.9	84.7
$(Sn)_xBi_{2-x}Te_3$:Sn-added			
x = 0.01	n	3.9	94.2
x = 0.03	p	2.4	102.4
$(Sn)_xBi_{2-x}Te_3$:Sn-substituted			
x = 0.01	n	1.1	171.7
x = 0.03	p	3.0	29.4
$(CuI + 1/2Sn)_xBi_2Te_3$:CuI/Sn-added			
x = 0.01	n	5.3	175.7
x = 0.03	n	9.6	90.5
x = 0.05	n	16.7	60.8
$(CuI + 1/2Sn)_xBi_{2-x}Te_3$:CuI/Sn-substituted			
x = 0.01	n	9.2	129.2
x = 0.03	n	13.2	81.4
x = 0.05	n	21.8	75.2

This behavior may be related to a decrease in the amount of electrically active defects presented in the sample upon doping with Sn. The 1 at.% Sn-added sample increased its carrier concentration, indicating that Sn acts as a donor ($n \approx 3.9 \times 10^{19}$ cm^{-3} for $Sn_{0.01}Bi_2Te_3$). However, the 1 at.% Sn-substituted sample had little effect on the net carrier concentration ($n \approx 1.1 \times 10^{19}$ cm^{-3} for $Sn_{0.01}Bi_{1.99}Te_3$), and therefore the physical properties. For CuI/Sn co-doped samples, the carrier concentration increases steadily by increasing the amount of CuI/Sn dopant from 5.3×10^{19} cm^{-3} to 16.7×10^{19} cm^{-3} for the CuI/Sn-added sample, and from 9.2×10^{19} cm^{-3} to 21.8×10^{19} cm^{-3} for the CuI/Sn-substituted samples. The mobility μ_H for CuI/Sn co-doped samples systematically decreased due to the increased scattering between carriers.

We selected Sn due to its unusual effect on the electrophysical properties of Bi_2Te_3 due to the formation of a resonance state in the allowed valence band [17]. Another reason for selecting Sn is to promote precipitation of Cu. Since the standard reduction potential of the Sn/Sn^{2+} couple (0.14 V) is less than that of the Cu^+/Cu^0 couple (0.52 V) [25], Sn can reduce Cu^+ ions to Cu^0 as follows:

$$2Cu^+ + Sn^0 \rightarrow 2Cu^0 + Sn^{2+}$$

The overall reaction can be written as

$$2CuI + Sn \rightarrow 2Cu + SnI_2$$

Therefore, Cu and SnI_2 precipitates form from the reduction of CuI with Sn in a high-temperature solid-state reaction, and the embedded precipitates can act as scattering centers in the CuI/Sn co-doped Bi_2Te_3 system.

The microstructures of the $(CuI/Sn)_{0.01}Bi_2Te_3$ samples were investigated by HRTEM. As shown in Fig. 2, the 1 at.% CuI/Sn co-doped Bi_2Te_3 was heavily nanostructured with various kinds of nanoprecipitates and lattice distortions dispersed throughout the Bi_2Te_3 matrix. HRTEM images (Fig. 2a, b) show coherently embedded nanoparticles of about 2–5 nm in the bulk matrix. The SAED pattern (Fig. 2b inset) taken along the [0001] direction indicates that the matrix possesses a Bi_2Te_3 type rhombohedral crystalline structure, and the precipitate regions showed extra atomic ordering (as indicated with open circles). In addition, CuI–Sn co-doped samples can readily identify abundant lattice defects, including dislocations and lattice distortion (Fig. 2c). An inverse fast Fourier transform (IFFT) image corresponding to Fig. 2d is presented in Fig. 2e, and it can be used to readily identify abundant dislocations and lattice distortions. The strain introduced by these dislocations is quantitatively analyzed using the geometrical phase analysis (GPA) method. The strain fields are represented by strain

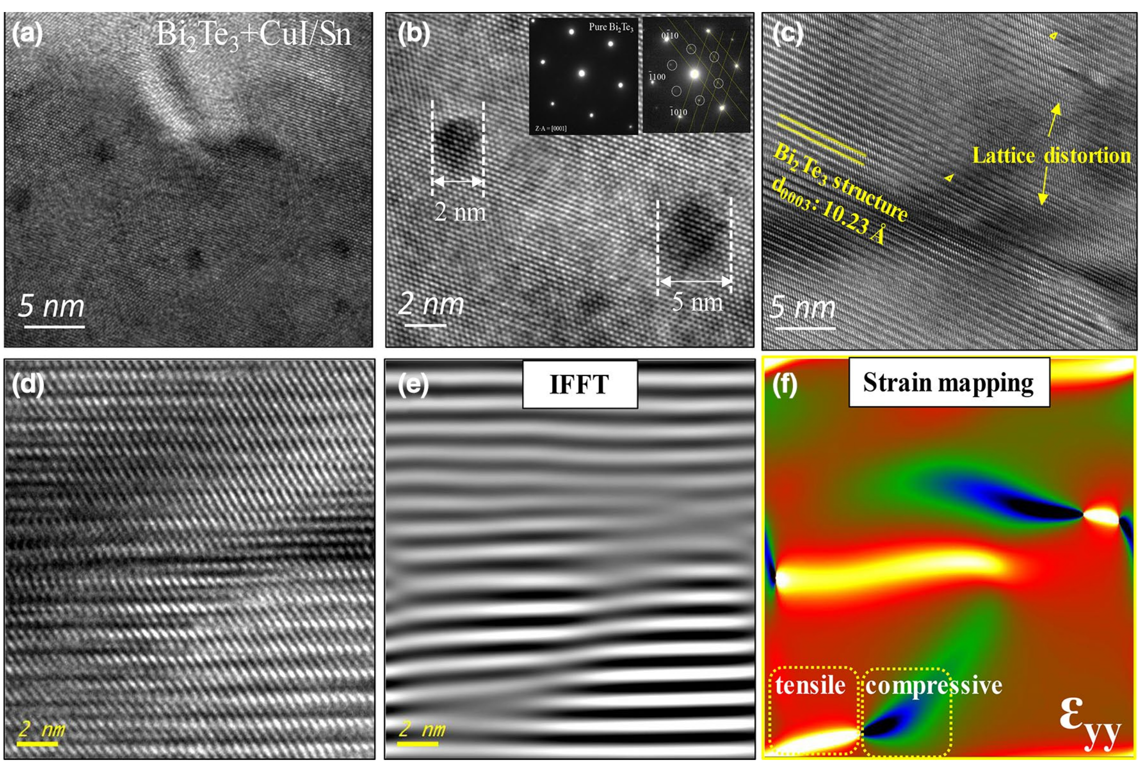

Fig. 2 **a** TEM images of CuI/Sn co-doped Bi_2Te_3. **b** HRTEM images depicting nanoprecipitates embedded in the Bi_2Te_3 matrix. The inset includes selected area electron diffraction (SAED) performed on various areas. **c** HRTEM micrographs of CuI/Sn co-doped Bi_2Te_3 **d** lattice defects, **e** an IFFT image corresponding to **d**, and **f** strain mapping corresponding to **d**

tensor components ε_{yy} as shown in Fig. 2f. The compressive and tensile stress is observed around the lattice distortion, which is thought to be caused by the co-doping of CuI and Sn elements.

The BF-TEM images of CuI/Sn co-doped Bi_2Te_3 are presented in Fig. 3, which more clearly shows the presence of two different phases of nanoprecipitates with bright and dark contrast in the Bi_2Te_3 matrix (marked with yellow and red circles). Although it was difficult to determine the actual composition of the nanoprecipitates using energy dispersive X-ray spectroscopy, we speculate that the nanoprecipitates are indeed Sn-I rich phases (marked by yellow circles) and Cu rich phases (marked by red circles). The addition of Cu and SnI_2 as nanoinclusions may introduce a carrier energy filtering effect as observed in other metallic nanoinclusions containing Bi_2Te_3-based materials [18, 26]. These nanosized precipitates in bulk Bi_2Te_3 will affect the electrical and thermal transport properties.

Figure 4 shows the temperature dependence of the thermoelectric properties for Sn-doped and CuI/Sn co-doped Bi_2Te_3. A pristine Bi_2Te_3 sample was also measured to examine the effect of doping on the electronic transport properties. The electrical conductivity at 300 K for Bi_2Te_3 was ~ 307 S cm^{-1}. The effect of Sn doping on the electrical conductivity of Bi_2Te_3 is more complex, as shown in Fig. 4a. Both the substitution of 1 at.% Sn for Bi^{3+} and addition of 1 at.% Sn in Bi_2Te_3 increased the electrical conductivity, while the electrical conductivity significantly decreased as the content of Sn increased to 3 at.%. These results suggest that Sn acts as a scattering center that disturbs electron conduction. With identical doping amounts, the singly Sn-substituted samples have much higher electrical conductivities than Sn-added samples. In the 1 at.% Sn-substituted sample, the electrical conductivity decreases with increasing temperature ($\delta\sigma/\delta T < 0$), following a power law of $\sigma \propto T^{-3/2}$. In contrast, the Sn-substituted sample with x = 0.03 and all cases of Sn-added samples displayed non-metallic behavior ($\delta\sigma/\delta T > 0$). Electrical conductivity decreased following a power law of $\sigma \propto T^{3/2}$, indicating that the carriers were predominantly scattered by ionized impurities (alloy disorder). The temperature dependence of the electrical conductivity for (CuI/Sn) co-doped Bi_2Te_3 samples is shown in Fig. 4b. All samples showed typical degenerated semiconductor-like behavior ($\delta\sigma/\delta T < 0$). Electrical conductivity decreased following a power law of $\sigma \propto T^{-3/2}$, indicating that the carriers were predominantly scattered by acoustic phonon scattering. No obvious bipolar conduction was observed. The electrical conductivity at room temperature for (CuI/Sn)-added Bi_2Te_3 samples showed a slight decrease with increasing (CuI/Sn) fraction. The electrical conductivity values ranged from 2193 to 2079 S cm^{-1}at 300 K. The electrical conductivity at room temperature for (CuI/Sn)-substituted Bi_2Te_3 samples showed an increase with increasing (CuI/Sn) content from 1 to 5 at.% and ranged from 2348 to 3797 S cm^{-1}. The values of electrical conductivity for (CuI/Sn)-substituted samples were larger than those of (CuI/Sn)-added samples. Here, σ is known to depend on the carrier concentration and mobility as shown in the relationship $\sigma = n\mu e$, where e is the carrier charge, n is the carrier concentration and σ is the mobility. As shown in Table 1, the carrier concentration

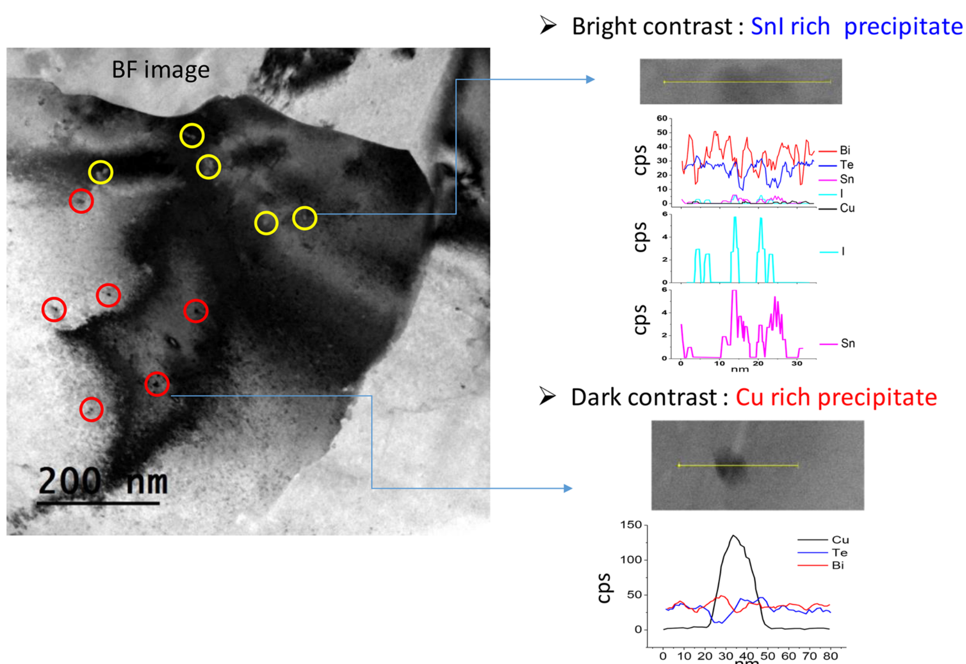

Fig. 3 BF-TEM images of CuI/Sn co-doped Bi_2Te_3 showing two different phases of nano-precipitate with bright and dark contrast in the Bi_2Te_3 matrix (marked with yellow and red circles). (Color figure online)

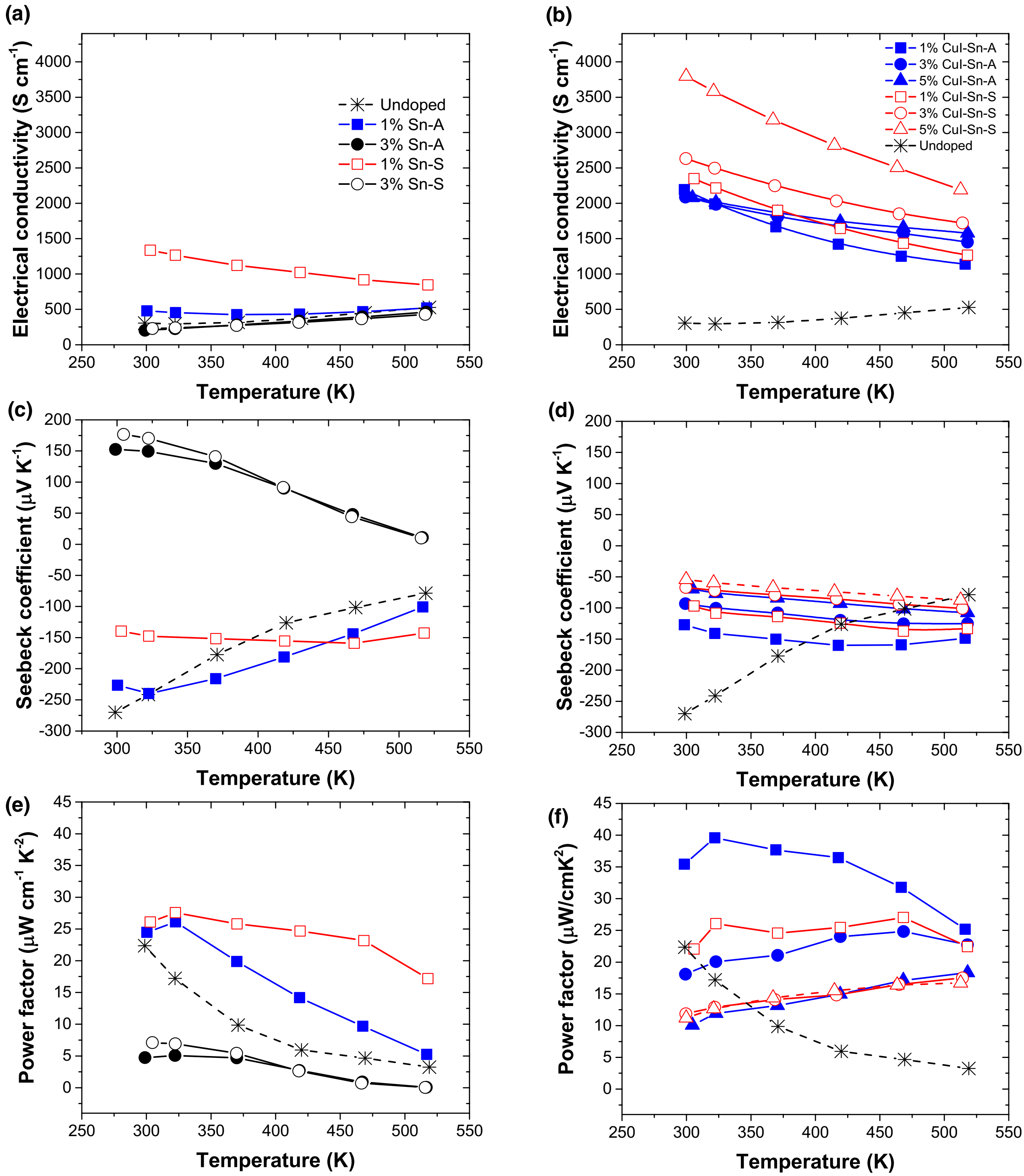

Fig. 4 Thermoelectric properties as a function of temperature for Sn-doped Bi_2Te_3 and CuI/Sn co-doped Bi_2Te_3 **a** and **b** electrical conductivity (σ), **c** and **d** Seebeck coefficient (*S*), **e** and **f** power factor. Here, *x*% Sn-A means $Sn_xBi_2Te_3$, *x*% Sn-S is $Sn_xBi_{2-x}Te_3$, *x*% CuI-Sn-A indicates the $(CuI+1/2Sn)_xBi_2Te_3$ sample, and *x*% CuI–Sn–S indicates the $(CuI+1/2Sn)_xBi_{2-x}Te_3$ sample

increased greatly as CuI/Sn content increased from 0 to 5 at.%. Figure 4 c and d show the temperature dependence of the Seebeck coefficients for Sn-doped and CuI/Sn co-doped Bi_2Te_3, respectively. The observed Seebeck coefficient values of Sn-doped specimens were negative for $x = 0.01$. They become positive for $x = 0.03$, which is consistent with the signs of the Hall measurements. This may be associated with the onset of the intrinsic behavior of Sn as a hole donor. According to conventional theory, the larger carrier concentration will lead to a smaller Seebeck coefficient. The magnitude of the Seebeck coefficient of the Sn-substituted sample decreased with increasing Sn content, whereas that of the Sn-added sample increased. These results are consistent with the trends of the Hall measurements. The Seebeck coefficients for CuI/Sn-co-doped samples were all negative for all the samples over the whole temperature range, indicating *n*-type conductors. This result is consistent with the negative values of the Hall measurement. As the (CuI/Sn)-co-doped amount increased from 1 to 3 at.%, the values of the Seebeck coefficients decreased due to the increased carrier concentration. As mentioned above, the carrier concentration increased significantly as the CuI/Sn co-doping content increased, thus causing a decrease in the Seebeck coefficient. All the samples showed similar temperature dependence of the Seebeck coefficient. The Seebeck coefficient values of all CuI/Sn co-doped samples exhibited a moderate decrease with increasing temperature. The temperature-dependent power factors ($S^2\sigma$) as a function of temperature for Sn-doped and CuI/Sn co-doped Bi_2Te_3 are shown in Fig. 4e and f, respectively. The power factor of the Sn-doped samples decreased with increasing doped Sn amount except around room temperature. The highest power factors of ~ 27.56 and ~ 26.11 μW cm^{-1} K^{-2} at 325 K were achieved for 1 at.% Sn-substituted and 1 at.% Sn-added Bi_2Te_3, respectively. The power factor for the CuI/Sn co-doped Bi_2Te_3 samples decreased with increasing doping content. A maximum power factor of ~ 35.4 μW cm^{-1} K^{-2} at 300 K was achieved for the 1 at.% CuI/Sn-added sample. This value is ~ 50% larger than that of the pristine Bi_2Te_3 (~ 22.4 μW cm^{-1} K^{-2} at 300 K) and the 1 at.% CuI/Sn-substituted Bi_2Te_3 sample (~ 22.1 μW cm^{-1} K^{-2} at 300 K).

To understand the effect of co-dopants, we compared the room-temperature Seebeck coefficient versus carrier concentration with the theoretical Pisarenko line [20, 27]. The data point for pristine Bi_2Te_3 fell on the Pisarenko line, demonstrating the validity of the adopted physical model. Except for the Sn-added samples, all samples showed higher Seebeck values than predicted by the Pisarenko line. As show in Fig. 5a, the Sn-substituted Bi_2Te_3 samples had much higher Seebeck coefficients than predicted by the Pisarenko relation, which was reported to arise from the resonant levels inside the valence band introduced by the Sn dopant [17, 28]. The Seebeck coefficients of Sn-substituted Bi_2Te_3 were very similar to previous values [17]. It was also revealed that CuI and Sn co-doped Bi_2Te_3 have slightly higher Seebeck coefficients at room temperature than predicted by the Pisarenko plot. If Sn or CuI is only a charge carrier regulator (pure dopant) in CuI/Sn co-doped Bi_2Te_3, then (CuI/Sn)-added and (CuI/Sn)-substituted Bi_2Te_3 should have the same Seebeck coefficients. However, this is not the case for the experimentally obtained results as shown in Fig. 5a. The Seebeck coefficients for the CuI and CuI/Sn-containing samples are high, as shown in Fig. 5a, indicating a higher effective mass, which is beneficial for the thermoelectric performance. We simply plotted the room-temperature power factor as a function of electron concentration, as shown in Fig. 5b. It is apparent that the CuI/Sn-containing samples showed significantly increased power factors, and the maximum values reached ~ 43 μW cm^{-1} K^{-2} for the $x = 0.01$ sample. The optimal electron concentrations for the power factor ranged from 5×10^{19} cm^{-3} to 6×10^{19} cm^{-3}.

A comparison of the temperature dependent thermoelectric properties for different dopants (CuI-doping, Sn-doping, and CuI/Sn co-doping) with 1 at.% doping concentration in Bi_2Te_3 is shown in Fig. 6. At identical doping fractions, the co-doping of CuI and Sn resulted in a higher improvement in the electrical conductivities due to the high carrier mobility and carrier concentration.

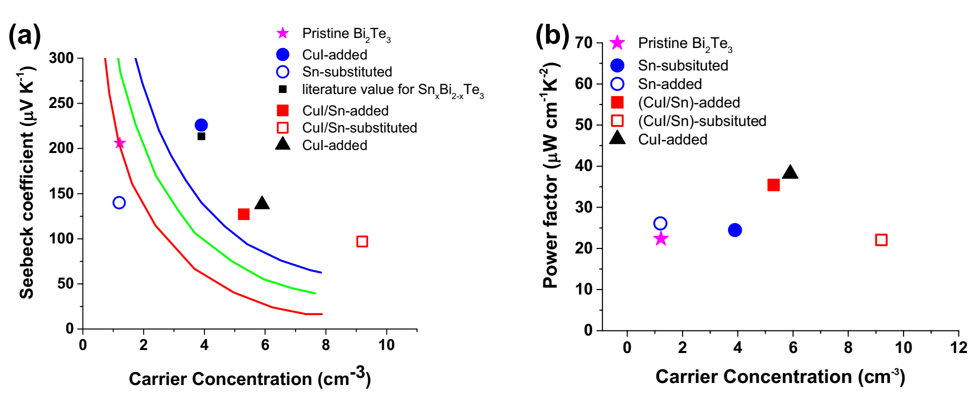

Fig. 5 Room-temperature **a** Seebeck coefficients (S) and **b** power factors as a function of carrier concentration (n) for Bi_2Te_3 with different dopants. The solid lines represent the Pisarenko relationships with different effective masses

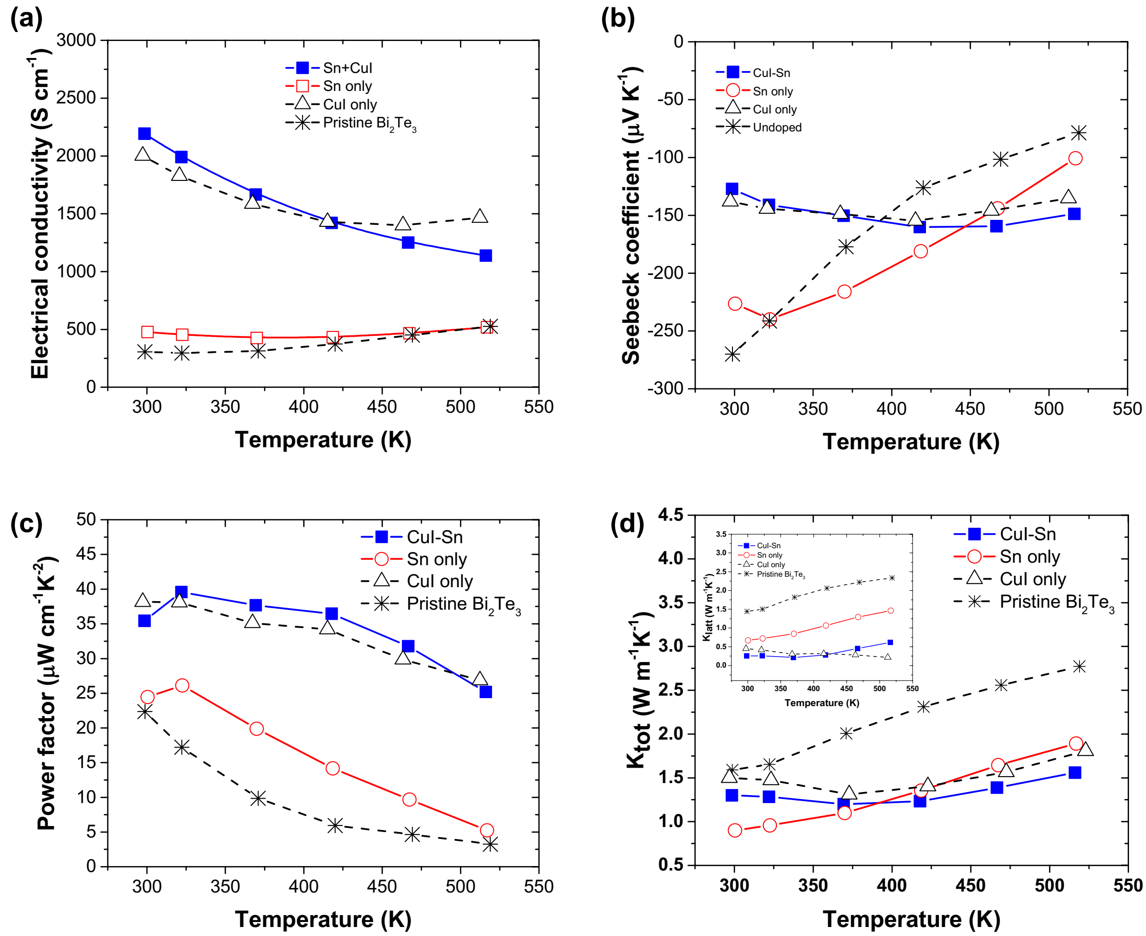

Fig. 6 The temperature dependence of **a** electrical conductivity (σ), **b** Seebeck coefficient (S), **c** power factor, and **d** thermal conductivity of x% CuI/Sn co-doped Bi_2Te_3 (x = 0.01, 0.03, 0.05, 0.07, and 0.10) including that for pristine Bi_2Te_3

Compared to pristine Bi_2Te_3, CuI-doping showed a donor effect and led to a substantial increase in the carrier concentration, thus increasing the electrical conductivity. As can be seen in Fig. 6b, the Seebeck coefficient showed a trend opposite to that of the electrical conductivity, which is strongly related to the carrier concentration. All samples with 1 at.% dopant concentration showed negative Seebeck coefficients, indicating that the samples were n-type semiconductors. The co-doped sample showed a room temperature Seebeck coefficient of -127.13 μV K^{-1}, which is lower than that of the CuI-doped sample ($S \sim -138.07$ μV K^{-1}). The temperature-dependent power factors ($S^2\sigma$) are shown in Fig. 6c as a function of temperature for Sn-doped, CuI-doped, and CuI/Sn co-doped samples. One can see that at the same doping level (~1 at.%), the power factors of CuI/Sn co-doped Bi_2Te_3 increased relative to single dopant doped Bi_2Te_3 and pristine Bi_2Te_3 over a very wide temperature range from 300 to 525 K. We evaluated the temperature dependences of the total (κ_{tot}) and lattice (κ_{latt}) thermal conductivity for Sn-doped, CuI-doped, and CuI/Sn co-doped Bi_2Te_3, as shown in Fig. 6d. As seen in Fig. 6d, the κ_{tot} for all doped samples is lower than that of the pristine sample. The κ_{tot} for pristine and Sn-doped Bi_2Te_3 gradually increased with increasing temperature. In the case of CuI-doped and CuI/Sn co-doped compounds, a slight upward curvature of κ_{tot} with temperature was observed at higher temperatures over 400 K. This behavior generally occurs in materials where n-and p-type carriers coexist [29]. The electronic contribution to the thermal transport is expected to be higher in the CuI/Sn co-doped sample due to the relatively high electrical conductivity values observed in the CuI/Sn co-doped compounds. However, the κ_{tot} of CuI/Sn co-doped sample was lower than that of single CuI-doped Bi_2Te_3 ($\kappa_{tot} \sim 1.44$ W m^{-1} K^{-1} for $(CuI + 1/2Sn)_{0.01}Bi_2Te_3$ and $\kappa_{tot} \sim 1.34$ W m^{-1} K^{-1} for $(CuI)_{0.01}Bi_2Te_3$). The reduction in the κ_{tot} for the CuI/Sn co-doped samples was mainly ascribed to the decreased lattice thermal conductivity. The total thermal conductivity (κ_{tot}) can be expressed as the sum of the lattice (κ_{latt})

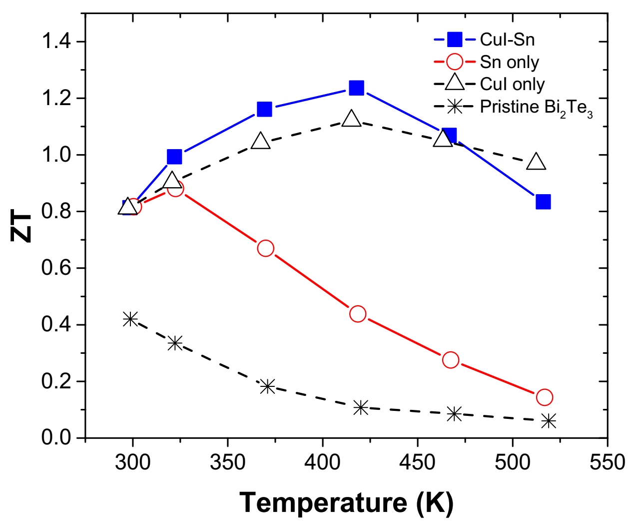

Fig. 7 Figure of merit of the Bi_2Te_3 with different dopants as a function of measurement temperature

and electrical thermal conductivity (κ_{elec}). κ_{elec} is proportional to the electrical conductivity according to the Wiedemann–Franz law ($\kappa_{elec} = L\sigma T$, where L is the Lorenz number ($L = 1.54 \times 10^{-8}$ V^2 K^{-2}) [30], σ is the electrical conductivity and T is absolute temperature). As seen from Fig. 6d, κ_{latt} of Sn-doped Bi_2Te_3 decreased by ~ 50% over the whole measured temperature range (300 K–525 K) compared to pristine Bi_2Te_3 (κ_{latt} ~ 1.44 W m^{-1} K^{-1} at 300 K). A further decrease in lattice thermal conductivity of CuI/Sn co-doped samples was observed, which may originate from an increase in point defect scattering after doping, as shown in the TEM analysis.

Figure 7 presents the temperature dependence of the dimensionless figure of merit (ZT) calculated from the combination of the electrical and thermal transport properties. The ZT values of all doped samples were significantly enhanced compared to pristine Bi_2Te_3 (ZT ~ 0.42 at room temperature). The ZT values of doped samples at room temperature were slightly changed by the added dopants. However, Sn-doping significantly increased the ZTs of Bi_2Te_3 in the low-temperature range (> 325 K), while the enhancement is marginal at elevated temperature. Compared to Sn-doped Bi_2Te_3, the ZT values of CuI-doped and CuI/Sn co-doped samples showed moderate temperature dependence over a wide temperature range (300 K–525 K). The maximum ZT value ~ 1.23 at 418 K was higher than that of Sn-doped Bi_2Te_3 (~ 0.88) and CuI-doped Bi_2Te_3 (~ 1.12). As shown in Fig. 7, co-doping of Sn and CuI causes an increase in the ZT in the mid temperature regions, which is probably due to the synergistic action of CuI and Sn. Our results suggest that further efforts to use co-dopant as an additive in bismuth telluride-based alloys would be promising for the development of high-performance *n*-type thermoelectric materials.

4 Conclusions

Co-doping effects of CuI and Sn on the thermoelectric properties of the Bi_2Te_3 matrix were investigated. Nanoprecipitates of the Cu and SnI-rich phase were generated by the reduction of CuI with Sn in the Bi_2Te_3 matrix. Numerous distinctive microstructures were revealed by TEM observation for the CuI/Sn co-doped samples, suggesting that such a bulk nanocomposite structure would be highly effective for reducing the thermal conductivity while maintaining high electrical conductivity. CuI/Sn co-doped Bi_2Te_3 showed a distinctly enhanced ZT value of 1.24 at 425 K, and the average ZT value (ZT_{ave} ~ 1.02) at 300–525 K was clearly higher than that in Sn-doped Bi_2Te_3 (ZT_{ave} ~ 0.54) and CuI-doped Bi_2Te_3 (ZT_{ave} ~ 0.98). Overall, we showed that significant progress in the thermoelectric performance of n-type Bi_2Te_3 can be achieved by employing a third element as a co-dopant with CuI to promote the precipitation of nanoinclusions.

Acknowledgements This research was supported by Nano Material Technology Development Program through the National Research Foundation of Korea (NRF) funded by the Ministry of Education, Science and Technology (NRF-2011-0030147). M.K.H. was supported by RP-Grant 2016 of Ewha Womans University.

Compliance with ethical standards

Conflict of interest There are no conflicts to declare.

References

1. D.M. Rowe, *Thermoelectrics Handbook: Macro to Nano* (CRC/Taylor & Francis, Boca Raton, 2006)
2. G. Tan, L. Zhao, M.G. Kanatzidis, Rationally designing high-performance bulk thermoelectric materials. Chem. Rev. **116**, 12123–12149 (2016)
3. L.E. Bell, Cooling, heating, generating power, and recovering waste heat with thermoelectric systems. Science **321**, 1457–1461 (2008)
4. L. Yang, Z.-G. Chen, M.S. Dargusch, J. Zou, High performance thermoelectric materials: progress and their applications. Adv. Energy Mater. **8**, 1701797 (2018)
5. Y. Lan, A.J. Minnich, G. Chen, Z. Ren, Enhancement of thermoelectric figure-of-merit by a bulk nanostructuring approach. Adv. Funct. Mater. **20**, 357–376 (2010)
6. S.I. Kim, K.H. Lee, H.A. Mun, H.S. Kim, S.W. Hwang, J.W. Roh, D.J. Yang, W.H. Shin, X.S. Li, Y.H. Lee, Dense dislocation arrays embedded in grain boundaries for high-performance bulk thermoelectrics. Science **348**, 109–114 (2015)
7. L.P. Hu, H.J. Wu, T.J. Zhu, C.G. Fu, J.Q. He, P.J. Ying, X.B. Zhao, Tuning multiscale microstructures to enhance thermoelectric performance of n-type bismuth-telluride-based solid solutions. Adv. Energy Mater. **5**, 1500411 (2015)

8. B. Zhu, Z.-Y. Huang, X.-Y. Wang, Y. Yu, L. Yang, N. Gao, Z.-G. Chen, F.-Q. Zu, Attaining ultrahigh thermoelectric performance of direction-solidified bulk n-type $Bi_2Te_{2.4}Se_{0.6}$ via its liquid state treatment. Nano Energy **42**, 8–16 (2017)
9. F. Hao, P. Qiu, Y. Tang, S. Bai, T. Xing, H.-S. Chu, Q. Zhang, P. Lu, T. Zhang, D. Ren, J. Chen, X. Shi, L. Chen, High efficiency Bi_2Te_3-based materials and devices for thermoelectric power generation between 100 and 300 °C. Energy Environ. Sci. **9**, 3120–3127 (2016)
10. H. Süssmann, A. Priemuth, U. Pröhl, Doping properties of Pb and Ge in Bi_2Te_2 and Sb_2Te_3. Phys. Status Solidi A **82**, 561–567 (1984)
11. I.V. Gasenkova, T.E. Svechnikova, Structural and transport properties of Sn-doped $Bi_2Te_{3-x}Se_x$ single crystals. Inorg. Mater. **40**, 570–575 (2004)
12. T.E. Svechnikova, P.P. Konstantinov, G.T. Alekseeva, Physical properties of $Bi_2Te_{2.85}Se_{0.15}$ single crystals doped with Cu, Cd, In, Ge, S, or Se. Inorg. Mater. **36**, 556–560 (2000)
13. G.E. Lee, I.H. Kim, Y.S. Lim, W.S. Seo, B.J. Choi, C.W. Hwang, Preparation and thermoelectric properties of doped Bi_2Te_3-Bi_2Se_3 solid solutions. J. Electron. Mater. **43**, 1650–1655 (2014)
14. Y. Xiao, J. Yang, Q.H. Jiang, L.W. Fu, Y.B. Luo, D. Zhang, Z.W. Zhou, Synergistic tuning of carrier and phonon scattering for high performance of n-type $Bi_2Te_{2.5}Se_{0.5}$ thermoelectric material. J. Mater. Chem. A **3**, 22332–22338 (2015)
15. S.-J. Jung, B.-H. Lee, B.K. Kim, S.-S. Lim, S.K. Kim, D.-I. Kim, S.O. Won, H.-H. Park, J.-S. Kim, S.-H. Baek, Impurity-free, mechanical doping for the reproducible fabrication of the reliable n-type Bi_2Te_3-based thermoelectric alloys. Acta Mater. **150**, 153–160 (2018)
16. F. Wu, H. Song, J. Jia, X. Hu, Effects of Ce, Y, and Sm doping on the thermoelectric properties of Bi_2Te_3 alloy. Prog. Nat. Sci. **23**, 408–412 (2013)
17. C.M. Jaworski, V. Kulbachinskii, J.P. Heremans, Resonant level formed by tin in Bi_2Te_3 and the enhancement of room-temperature thermoelectric power. Phys. Rev. B **80**, 233201 (2009)
18. Q. Zhang, X. Ai, L. Wang, Y. Chang, W. Luo, W. Jiang, L. Chen, Improved thermoelectric performance of silver nanoparticles-dispersed Bi_2Te_3 composites deriving from hierarchical two-phased heterostructure. Adv. Funct. Mater. **25**, 966–976 (2015)
19. M.-K. Han, K. Ahn, H.J. Kim, J.-S. Rhyee, S.-J. Kim, Formation of Cu nanoparticles in layered Bi_2Te_3 and their effect on ZT enhancement. J. Mater. Chem. **21**, 11365–11370 (2011)
20. S. Wang, H. Li, R. Lu, G. Zheng, X. Tang, Metal nanoparticle decorated n-type Bi_2Te_3-based materials with enhanced thermoelectric performances. Nanotechnology **24**, 285702 (2013)
21. M.-K. Han, B.G. Yu, Y. Jin, S.-J. Kim, A synergistic effect of metal iodide doping on the thermoelectric properties of Bi_2Te_3. Inorg. Chem. Front. **4**, 881–888 (2017)
22. B.A. Hunter, C.J. Howard, *Rietica* (Australian Nuclear Science and Technology Organization: Menai, 1998) http://www.ccp14.ac.uk/tutorial/lhpm-rietica/doc/manual.pdf
23. W. McClune, Powder Diffraction File, JCPDS-International Center for Diffraction Data, Swarthmore, PA. http://www.icdd.com/index.php/pdfsearch/
24. Y.S. Lim, M. Song, S. Lee, T.-H. An, C. Park, W.-S. Seo, Enhanced thermoelectric properties and their controllability in p-type $(BiSb)_2Te_3$ compounds through simultaneous adjustment of charge and thermal transports by Cu incorporation. J. Alloys Compd. **687**, 320–325 (2016)
25. D.R. Lide, *CRC Handbook of Chemistry and Physics*, 90th edn. (CRC Press, Boca Raton, 2009)
26. S. Sumithra, N.J. Takas, D.K. Misra, W.M. Nolting, P.F.P. Poudeu, K.L. Stokes, Enhancement in thermoelectric figure of merit in nanostructured Bi_2Te_3 with semimetal nanoinclusions. Adv. Energy Mater. **1**, 1141–1147 (2011)
27. A.F. Ioffe, *Physics of Semiconductors* (Academic Press, New York, 1960)
28. B. Wiendlocha, Resonant levels, vacancies, and doping in Bi_2Te_3, Bi_2Te_2Se, and Bi_2Se_3 tetradymites. J. Electron. Mater. **45**, 3515–3531 (2016)
29. J.S. Rhyee, E. Cho, K.H. Lee, S.M. Lee, S.I. Kim, H. Kim, Y.S. Kwon, S.J. Kim, Thermoelectric properties and anisotropic electronic band structure on the In_4Se_{3-x} compounds. Appl. Phys. Lett. **95**, 212106 (2009)
30. H.-S. Kim, Z.M. Gibbs, Y. Tang, H. Wang, G.J. Snyder, Characterization of Lorenz number with Seebeck coefficient measurement. APL Mater. **3**, 041506 (2015)